Climatology of Hail Frequency and Size in China, 1980–2015

XIAOFEI LI, QINGHONG ZHANG, TIAN ZOU, JIPEI LIN, AND HOIIO KONG

Department of Atmospheric and Oceanic Sciences, School of Physics, Peking University, Beijing, China

ZHIHUA REN

National Meteorological Information Center, China Meteorological Administration, Beijing, China

(Manuscript received 24 July 2017, in final form 26 January 2018)

ABSTRACT

The hail day climatology from 1961 to 2005 was previously studied based on hundreds of surface stations in China. Recently, both hail occurrence and maximum hail diameter (MHD) data from more than 2000 surface stations were released by the National Meteorological Information Center of China. These data enable hail climatology to be explored using both hail frequency (HF), which is defined as annual mean hail occurrence, and MHD records from more stations over the entire country. Following quality control, hail data from 2254 stations were selected for the period of 1980–2015. In general, HF increased with station topography height, with a maximum of more than 30 events per year in the Tibetan Plateau and a minimum of less than 1 event per year in southern China, whereas the station mean MHD decreased with topography height. The highest peak of the 80th-percentile cumulative distribution function of the annual MHD cycle in southern China occurred in May but was delayed to July in the north. Severe hail (MHD $\geq$ 20 mm; 5.32% of all cases) mainly occurred along the edge of the plain, near the mountainsides, and was most likely to develop in the afternoon.

1. Introduction

The natural hazard of hail is generally produced by deep convective storms with an appropriate updraft strength, sufficient supercooled liquid water content, conducive temperature conditions, and an optimal lifetime (Nelson 1983; Ziegler et al. 1983; Hohl et al. 2002; Grant and van den Heever 2014; Punge and Kunz 2016; Dennis and Kumjian 2017; Li et al. 2017). Hail often develops during a short time period (as little as a few minutes and up to a few hours), directly causing huge economic and human losses on a daily scale in China (Cao 2008; Guan et al. 2015; Li et al. 2017). The substantial impacts of hail on agriculture, ecosystems, and human society can last over time scales from months to seasons. In 2015, for example, 57 people were killed directly by hailstorms, 0.67 million houses were damaged, 2.92 million ha of crops were affected, and CNY 32.27 billion of direct economic loss occurred because of severe storms, including hailstorms, tornadoes, and damaging winds (China Meteorological Administration 2016). Therefore, understanding the accurate climatology of hail is the first step toward improving hail disaster prevention strategies.

The climatology of hail has been studied using various types of data over different spatial and temporal scales worldwide (Vinet 2001; Schuster et al. 2005; Tuovinen et al. 2009; Cintineo et al. 2012; Kim and Ni 2014; Burcea et al. 2016; Kahraman et al. 2016; Punge and Kunz 2016; Martins et al. 2017). For example, in Europe, hail risk has been determined using data from 1987 to 1996 from a hail pad network and insurance data (Vinet 2001). Hail climatology has also been explored using the data from newspapers, storm spotters, and eyewitness reports during a relatively long period (1930–2006) in Finland from the perspective of severe hail days and hail size distribution (Tuovinen et al. 2009). Both hail days and hail size have been studied by using data from 105 weather stations in Romania during 1961–2014 (Burcea et al. 2016). A comprehensive review of hail climatology in Europe has been presented by Punge and Kunz (2016). In North America, hail days were recently studied in the United States using multiradar multisensor data for only 4 years, during 2007–10 (Cintineo et al. 2012), and hail

Corresponding author: Prof. Qinghong Zhang, qzhang@pku.edu.cn

DOI: 10.1175/JAMC-D-17-0208.1

© 2018 American Meteorological Society. For information regarding reuse of this content and general copyright information, consult the AMS Copyright Policy (www.ametsoc.org/PUBSReuseLicenses).

Unauthenticated | Downloaded 05/15/25 05:17 PM UTC

size was also studied from hail reports during 1955–2014 (Allen and Tippett 2015; Allen et al. 2017). In South America, hailstorm frequency has been studied in Brazil using data based on reports collected during a 22-yr period, from 1991 to 2012 (Martins et al. 2017). In Australia, hailstorm frequency and maximum hail size have been studied using data from reports between 1791 and 2014 (Schuster et al. 2005; Allen and Allen 2016). In addition, in western Asia, the climatology of severe hail has been studied in Turkey using data from meteorological stations, newspaper archives, and Internet sources during 1925–2014 (Kahraman et al. 2016). In East Asia, the climatology of hail days has been studied on the Korean Peninsula using data collected by meteorological stations during the past four decades (Kim and Ni 2014; Jin et al. 2017). Hail climatology is typically studied in China using meteorological station records (Liu and Tang 1966; Zhang et al. 2008; Xie et al. 2008, 2010; Li et al. 2016; Ni et al. 2017) and satellite data (Ni et al. 2016).

Global severe hail maps have been produced from various indirect observations, including global model analysis data and satellite retrieval data (Hand and Cappelluti 2011; Cecil and Blankenship 2012). Hand and Cappelluti (2011) generated a global hail climatology with a minimum threshold of 15 mm by diagnosing 5-yr global model data, which overcame the difficulties of the high frequency of hail days in areas of high orography. Cecil and Blankenship (2012) estimated an 8-yr climatology of large hailstones (minimum threshold of 25 mm) from satellite measurements, which showed an overestimation in the tropics because of the satellite proxy for hail frequency or the limited number of hail observations in these areas. These differences cannot be further explored until hail sizes derived from satellite data and model outputs are compared with reliable surface-based observations.

Hail can occur almost everywhere, and the hail season has a diverse geographical distribution in China (Zhang et al. 2008; Ni et al. 2017). Hail day frequency in northern China is typically higher than that in southern China (Li et al. 2016). Most studies have focused mainly on the climatology and long-term trends of hail, from the perspective of the hail days, using data from hundreds of stations. These studies have usually disregarded hail size because different provincial meteorological bureaus kept hail size records individually until 2016, although Liu and Tang (1966) collected hail size data from 60 stations during 1951–62. The climatology of hail size was studied by Xie et al. (2010) in four subareas in China using data from only 146 stations, who found that Guizhou Province (in southwestern China) had the largest proportion of severe hailstones greater than 15 mm. The patterns of hail frequency and hail size distribution in China remain unclear. Recently, hail data from surface observations were released by the National Meteorological Information Center (NMIC) of China for the period of 1954–2015, from more than 2000 stations in mainland China, including occurrence time and maximum hail diameter (MHD), producing one of the most complete and uniform hail datasets currently available in the world. The availability of these new data provides an opportunity to analyze hail frequency (HF) from a large number of stations and the climatology of hail size for the entire country. These new analyses will improve our understanding of the climatology of hail in China.

This study focused on the spatial distribution of HF and MHD in China and their annual and diurnal cycles regardless of interannual long-term trends or the linkage of environmental conditions. The details of the dataset and definitions are provided in section 2. Sections 3 and 4 present the results of the analysis of hail and severe hail records, respectively, with the conclusions provided in section 5.

2. Data and definitions

The comprehensive historical hail dataset from the NMIC included 2477 stations in mainland China from 1954 to 2015. A standard hail precipitation record contains the start and end time of one hail event in daytime (0800–1959 LT) and the MHD if it equals or exceeds 2 mm, along with the properties of rebound resilience and nonfrangibility. The exact start and end times of hail events at night (2000–0759 LT) are not recorded at general observation stations, but the MHD is, according to the observational guide of China (China Meteorological Administration 2007). If a hail event is recorded at one station, it is reported as a hail occurrence for that station. If the time interval between two hail events at one station is more than 15 min, they are treated as two hail occurrences. Every station reported the hail characteristics at the local or county scale surrounding the station. However, hail size was not routinely recorded until 1980, when the new observational guide for meteorological stations was implemented (Xie et al. 2010). Thus, the period considered in this study was limited to 1980–2015. HF was defined as the annual mean hail occurrence for a given weather station during 1980–2015. To ensure a relatively large and continuous dataset, if observations were missing for a period of one month or more or if there was no hail record at a station, then that station was regarded as invalid. As a result, 2254 stations with continuous observations from 1980 to 2015 were selected.

Unauthenticated | Downloaded 05/15/25 05:17 PM UTC

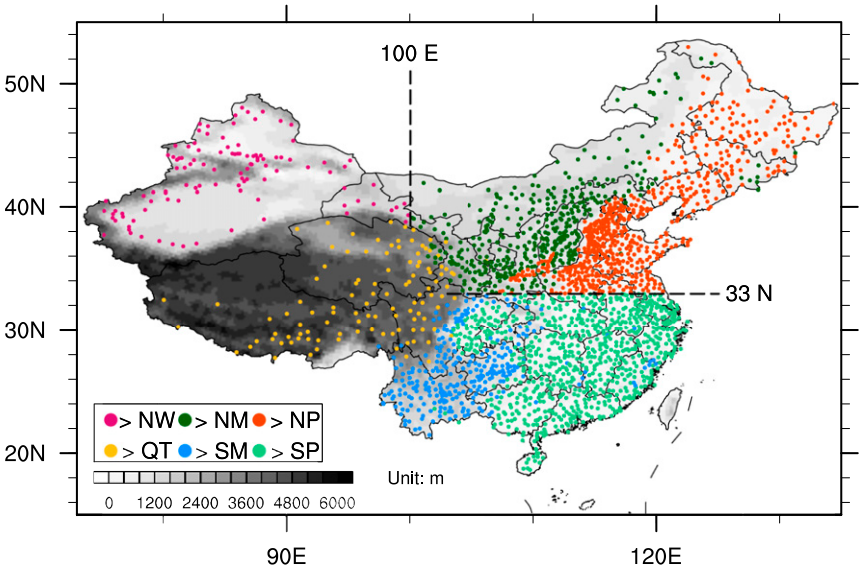

FIG. 1. Geographic distribution of 2254 meteorological observational stations with topography in China, divided into six subareas. Purple: NW; deep green: NM; red: NP; yellow: QT; blue: SM; light green: SP.

Because hail day occurrence is highly dependent on the geographical distribution and different synoptic systems develop from west to east and from north to south in China (Liu and Tang 1966; Zhang et al. 2008; Xie et al. 2008, 2010; Li et al. 2016; Ni et al. 2017), six subareas were defined for this study (Fig. 1). The Qinghai–Tibet Plateau (QT) was defined by the altitude of stations with elevation equal to or higher than 2500 m, south of 40°N and west of 105°E, with 32 120 hail occurrence records and 24 289 MHD records from 110 stations. The northwest area (NW) was defined as the area to the north of QT and west of 100°E, having 4197 hail occurrence records and 3126 MHD records from 108 stations. The remaining area was divided into four subareas (the dividing lines were 33°N and 500-m altitude), including the northern mountain area (NM) with 19 362 hail occurrence records and 15 444 MHD records from 381 stations, the northern plain area (NP) with 14 742 hail occurrence records and 11 534 MHD records from 609 stations, the southern mountainous area (SM) with 9971 hail occurrence records and 6032 MHD records from 283 stations, and the southern plain area (SP) with 7106 hail occurrence records and 4570 MHD records from 763 stations (Table 1). This subarea scheme was more detailed than that created by Li et al. (2016) because of the inclusion of topographic height as a criterion and the large number of stations. Of the total records, 511 (0.79%) were converted from descriptive sizes (e.g., ''beans,'' ''eggs,'' and ''ping-pong balls'') to approximate numeric values among 64 815 hail size records, according to a quality-controlled classification used by NMIC (Table 2). This was because some exact measurements of hail size records were missing and reference object metadata were used instead.

In this study, severe hail was defined as an event with an MHD equal to or greater than 20 mm, to make this dataset comparable with those produced in other parts of the world. For example, in the United States, severe hail was defined by the National Weather Service (NWS) to have a threshold diameter of 0.75 in. (approximately 19 mm) (Johns and Doswell 1992) and was redefined to 1.00 in. (approximately 25 mm) by the NWS, which Allen and Tippett (2015) subsequently used. In Europe, the threshold diameter was defined as 20 mm or greater on the longest axis or smaller hailstones forming a 20-mm layer on flat parts of Earth's surface (Brooks and Dotzek 2008; Dotzek et al. 2009). However, some previous studies defined the threshold of severe hail as 15 mm, for example, in Turkey (Kahraman et al. 2016) and in four regions of China, because of the limited number of larger hail records (Xie et al. 2010).

3. Hail climatology

As described in the previous section, the climatological features of hail days and their patterns in China have been studied frequently (Liu and Tang 1966; Zhang et al. 2008; Xie et al. 2008, 2010; Li et al. 2016). However, there are few consistent datasets containing both MHD and HF. It should be given greater attention in studies using the comprehensive dataset described in section 2.

Unauthenticated | Downloaded 05/15/25 05:17 PM UTC

TABLE 1. Hail occurrence and MHD records for hail and severe hail events in six subareas.

	Subareas	NP	NM	NW	QT	SM	SP	Total
All hail records	Station number	609	381	108	110	283	763	2254
	Number of records with hail occurrence	14 742	19 362	4197	32 120	9971	7106	87 498
	Number of records with MHD	11 534	15 444	3126	24 289	6032	4570	64 815
Severe hail records	Station number	467	289	43	66	176	405	1446
	Record number	1166	845	92	221	463	660	3447

There were 64 815 hail size records (74.08%) among 87 498 hail occurrence records collected from 2254 meteorological observational stations during 1980–2015 (Table 1).

a. Spatial distribution of hail events

The spatial distribution of HF and its relationship with elevation are shown in Fig. 2. The annual climatology map very clearly shows the HF features from 1980 to 2015, with greater HF values over mountainous areas. This observation is similar to those of previous climatology studies of hail day number from station observations (Liu and Tang 1966; Zhang et al. 2008; Xie et al. 2008, 2010; Li et al. 2016). The highest HF values were concentrated in the center of the QT, and the second highest values occurred in NM. The highest HF value during 1980–2015 was 37.6 per year at Naqu station (No. 55299; altitude: 4507 m) in QT. Hail occurred more frequently in northern China than in southern China and more frequently in mountainous areas than in plains areas. HF

TABLE 2. Approximate hailstone diameter, as interpreted from hail record descriptions.

Description	Approx diameter (mm)	Description	Approx diameter (mm)
Basketball	250	Sichuan bean	20
Rice bowl	100	Copper buttons	20
Steamed bun	100	Glass ball	20
Pear	80	Camphor ball	20
Persimmon	80	Coin	15
Apple	80	*Vicia faba*	15
Peach	80	Abacus counter	15
Goose egg	80	Apricot pit	15
Fist	80	Lima bean	15
Billiard ball	80	Button	10
Duck egg	60	Fingernail	10
Chicken egg	60	Little finger	10
Camel dung	60	Apricot kernel	10
Ping-pong ball	40	Peanut	10
Plum	40	Wild jujube	10
Chinese chess piece	40	Gorgon fruit	10
Large walnut	40	Hyacinth bean	10
Apricot	30	Stump of pencil	10
Small chicken egg	30	Stump of chopsticks	10
Tangyuan	30	Dwarf bean	10
Glutinous rice cake	30	Soybean	8
Spadger egg	30	Red bean	8
Pigeon egg	30	Pea	8
Egg yolk	30	Corn kernel	8
Small walnut	20	Cotton seed	8
Thumb	20	Black bean	8
Red date	20	Castor seed	5
Bowl of long-stemmed pipe	20	Mung bean	5
Chestnut	20	Adzuki bean	5
Hawthorn	20	Petai	5
Longan	20	Coarse salt	5
Hazelnut	20	Grain of rice	5
Date plum persimmon	20	Grain of wheat	5
Ginkgo	20	Chinese sorghum grain	3
Acorn	20	Millet grain	2

Unauthenticated | Downloaded 05/15/25 05:17 PM UTC

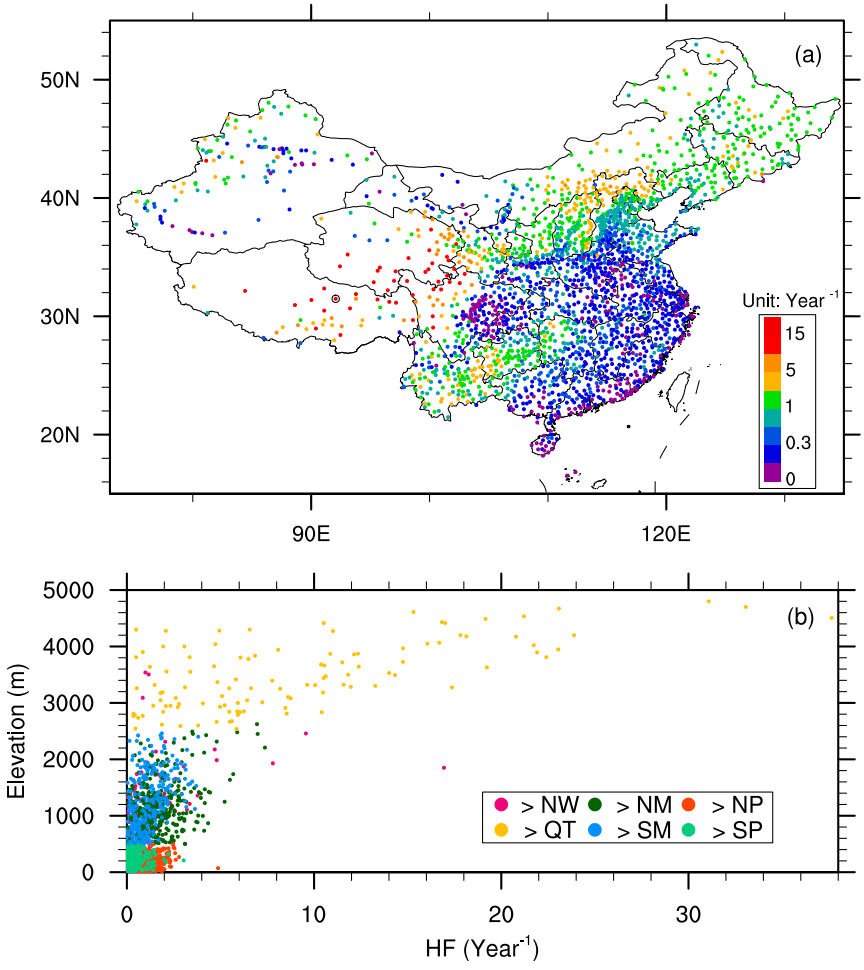

FIG. 2. (a) Distribution of annual mean HF at the stations shown in Fig. 1 from 1980 to 2015. Naqu station (55299; 31.5°N, 92.1°E; hollow circle) recorded the highest value (37.6 times per year) during this period in QT. (b) HF vs elevation (m), with the color symbols identified in Fig. 1.

exhibited a sharp gradient at the edge of the plains areas, near the boundary with the mountainous areas.

In contrast, the mean MHD increased from west to east and from north to south with obvious regional differences (Fig. 3a). The station mean MHD records were all less than 20 mm in QT. Most station mean MHD records were below 20 mm and only a small group exceeded 20 mm, in NM, NW, and SM. However, most station mean MHD records equal to or exceeding 20 mm were found in SP and NP where the HF pattern was nearly the opposite of that of topographic height. In general, the mean MHD increased from plateaus to mountainous areas and increased further to the plains areas, with a wider range of the mean MHD from higher to lower elevation areas (Fig. 3c).

Similarly, the maximum value of MHD at each station during 1980–2015 also increased from west to east and from north to south (Fig. 3b). No station recorded a maximum MHD larger than 100 mm in the central area of the QT during the study period. Stations with maximum MHD equal to or greater than 100 mm were mainly located in SP and NP, distributed irregularly along their edges, near the border with the mountainous areas.

Although hail events occurred almost everywhere in China, the probability distribution function (PDF) of MHD displayed some differences among the six subareas (Fig. 4). Most hail events were distributed into the 2- and 3-mm bins in QT and in the 5-mm bin in the other five subareas. The plains area received a greater percentage of severe hail events than the mountainous area, and southern China received a greater percentage of severe hail events than northern China. The QT had the lowest number of severe hail events of the six subareas. HF closely followed the topography, while the MHD was inversely related to topographic height. This result may be explained by high topography providing a

Unauthenticated | Downloaded 05/15/25 05:17 PM UTC

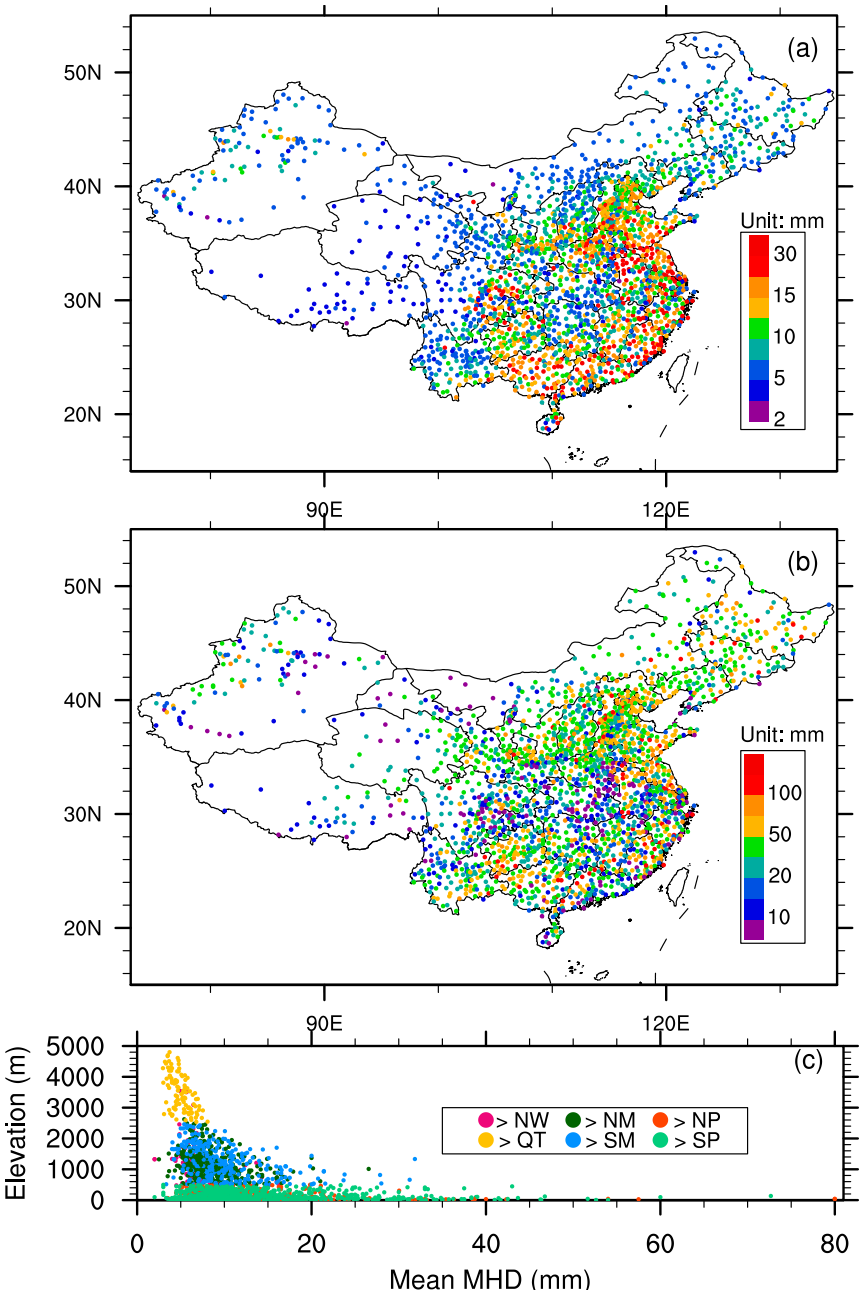

FIG. 3. Distribution of (a) mean MHD and (b) maximum MHD at the stations shown in Fig. 1 from 1980 to 2015. (c) Mean MHD (mm) vs elevation (m) with the color symbols identified in Fig. 1.

favorable environment for air lifting with a relatively low freezing height to form convective storms in the warm season, contributing greatly to larger HF values in mountainous areas (Changnon 1978; Changnon and Changnon 2000; Li et al. 2016). However, plains areas provided a favorable environment for convective available potential energy (CAPE), with more water vapor, but a higher freezing height than topographic height, to form stronger convection in spring and autumn, contributing more to MHD growth (Thielen and Gadian 1997; Xie et al. 2010; Yu et al. 2016; Li et al. 2016; Zheng et al. 2016). Sufficient vertical wind shear also supported convection formation, increasing the risk of large hailstones (Xie et al. 2008; Punge and Kunz 2016), which was found to be induced mostly by monsoons in southern China (Li et al. 2013).

Unauthenticated | Downloaded 05/15/25 05:17 PM UTC

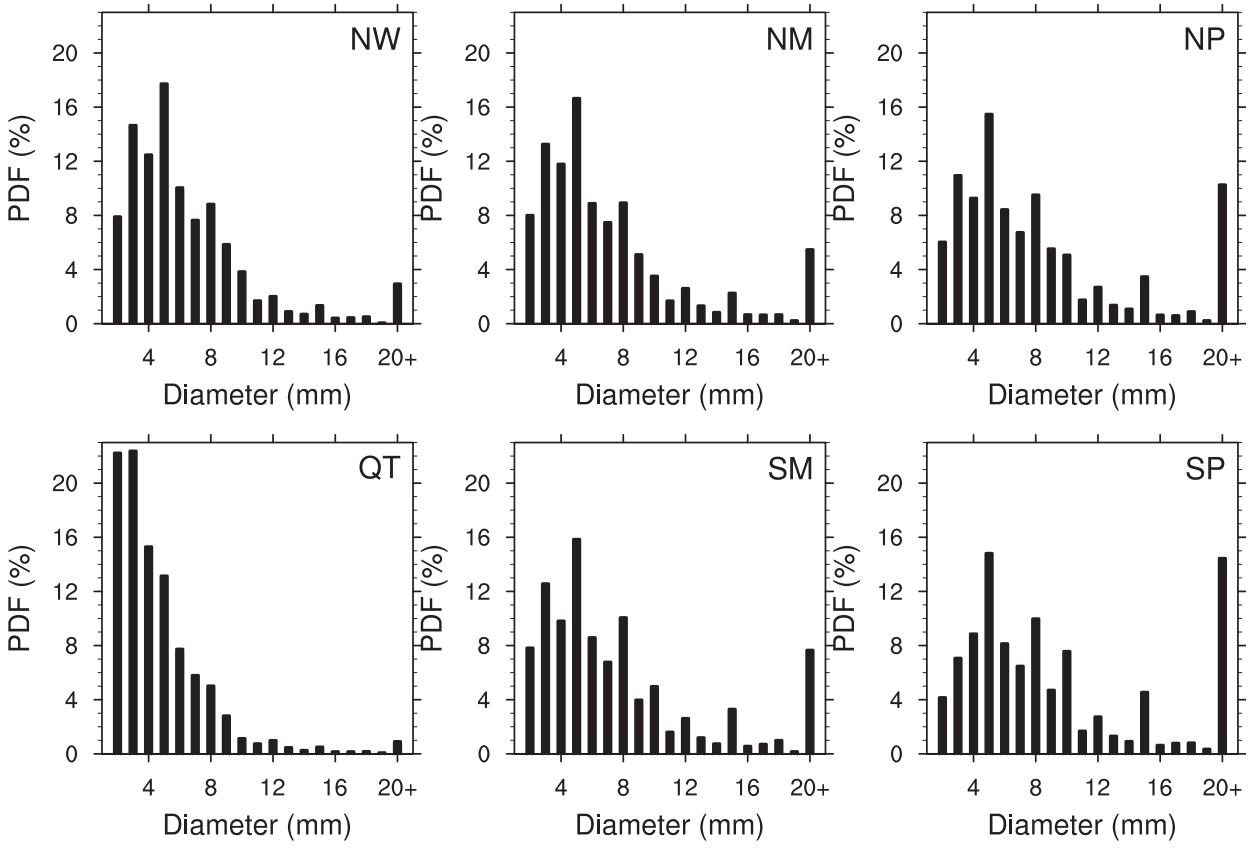

FIG. 4. PDFs of MHD in the six subareas shown in Fig. 1 from 1980 to 2015.

b. Annual cycle

Hail can occur throughout the year, as revealed by the annual hail distribution, but with different patterns among the six subareas (Fig. 5). The hail season starts in southern China in spring when the summer monsoon forms over the southern coast and then moves to north China in summer as the summer monsoon extends to the north of the country (Zhang et al. 2008). There were no hail occurrence records in the NW region from November to February, and only a few events were recorded in NM, NP, and QT during the cold season. The vast majority of hail events occurred during April–October in NW, NM, NP, and QT, and the peak months for HF in SM and SP were April and March, with 26% and 36% of the annual hail occurrence, respectively. June is the peak month for HF in NW, NM, NP, and QT, with more than 20% of the annual hail events, which is consistent with a previous finding that southern China experiences hail earlier than the rest of the country during the calendar year (Zhang et al. 2008; Li et al. 2016).

Although some previous articles have presented the seasonal variation in hail day frequency in China (Zhang et al. 2008; Xie et al. 2010; Li et al. 2016), few works have presented the annual cycle of HF together with MHD. To improve our understanding of MHD variation and to exclude extreme values over the annual cycle, a cumulative distribution function was calculated; 80th-, 50th-, and 20th-percentile values are presented in Fig. 5. The annual variation in MHD roughly followed that in HF during the same period with a 1–2-month lag in all subareas except QT. Annual MHD varied very little from June to September in QT, where the 50th percentile fluctuated around 4 mm. The 50th percentile reached a peak of 6 mm in June in NW, fitting the same HF peak month and remaining at 5 mm in months between March and October. In both NM and NP, the 80th-percentile CDF peaked in July, which was delayed by 1 month relative to that of HF in these two subareas. The peaks of the 80th-percentile SP and SM were both in May, and the difference between the 80th and 20th percentiles of the CDF was enhanced greatly in SP. The 80th percentile of the CDF trend began with a steady increase from January and reached its first and highest peak of 23 mm in May. There were two peak periods in SP, from April to June and from August to October. The first 80th percentile of CDF and 50th percentile of CDF peaks in SM were delayed by 1 month relative to the peak HF values and were delayed by 2 months in SP.

Unauthenticated | Downloaded 05/15/25 05:17 PM UTC

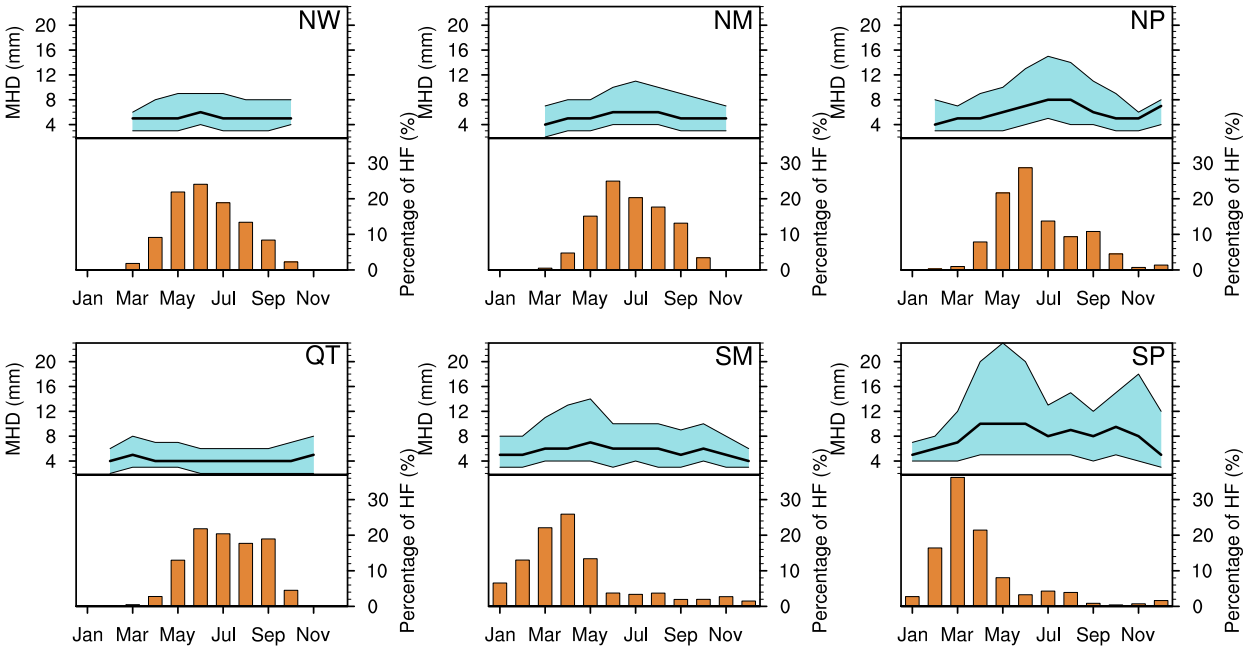

FIG. 5. Annual MHD (line graphs) and mean percentage HF (bar charts) for the six subareas shown in Fig. 1. The upper black lines indicate the MHD reaching the 80th percentile of the CDF; the lower black lines indicate the MHD reaching the 20th percentile of the CDF; thick black lines indicate the MHD reaching the 50th percentile of the CDF.

These results suggest that HF and MHD are affected by both topography and atmospheric circulation and may be related to atmospheric variation favoring different types of hail growth in different subareas. For example, the distribution of HF might be determined by the distribution of freezing-level height and air lifting, typically experienced in hail-favoring atmospheric circulation systems like frontal systems and cutoff lows in mountainous areas in spring and fall. However, the determination of MHD has been given less consideration and is not very clear in China, although the importance of freezing-level height and column cloud liquid water on hail size have been assessed by a one-dimensional model (Xie et al. 2010). Further, the East Asian summer monsoon, the primary source of moisture and dynamic forcing conducive to warm-season severe weather, exhibiting a northeastward progression over China, performs quite differently in different subareas; this dynamic might also play a role in determining both the spatial and temporal distribution of MHD and HF (Zhang et al. 2008; Zhang et al. 2017).

c. *Diurnal cycle*

Hail can occur during all hours of the day, with a considerable diurnal cycle, and occurred more frequently in daytime (except mornings) in all six subareas (Fig. 6). In all subareas, the highest percentage of HF in the diurnal cycle occurred during the afternoon, which is similar to the finding of a previous study (Zhang et al. 2008). The peak is mainly a result of surface heating resulting from solar radiation in the diurnal cycle, as solar radiation processes destabilize the atmospheric column, favoring the development of ordinary daytime convection and enhancing existing convective systems (Zhang et al. 2008). The percentage of morning HF was slightly higher than at night in northern China in both the plains and mountainous areas. However, the percentage of HF at night was higher in the south, where vortices occur more frequently at night (X. Chen et al. 2014). Hailstorms were elevated and formed later in the day on the favorable lifting trajectories, induced by the low-level jet strengthening during the evening and night and nocturnal elevated convection (G. Chen et al. 2014; Li et al. 2015).

The diurnal cycle of MHD is displayed in box plots in Fig. 6, excluding extreme records; the 95th percentile of the CDF value was used as the maximum MHD and the 5th percentile of the CDF value was used instead of the minimum. These plots show that the peaks in MHD during the diurnal cycle were delayed relative to those in HF in all subareas, with the highest 95th percentile during the evening and the highest 75th percentile in evening except in SP. The peak of the 50th percentile of CDF lines occurred later in the evening in SM than it occurred in the afternoon in SP.

Unauthenticated | Downloaded 05/15/25 05:17 PM UTC

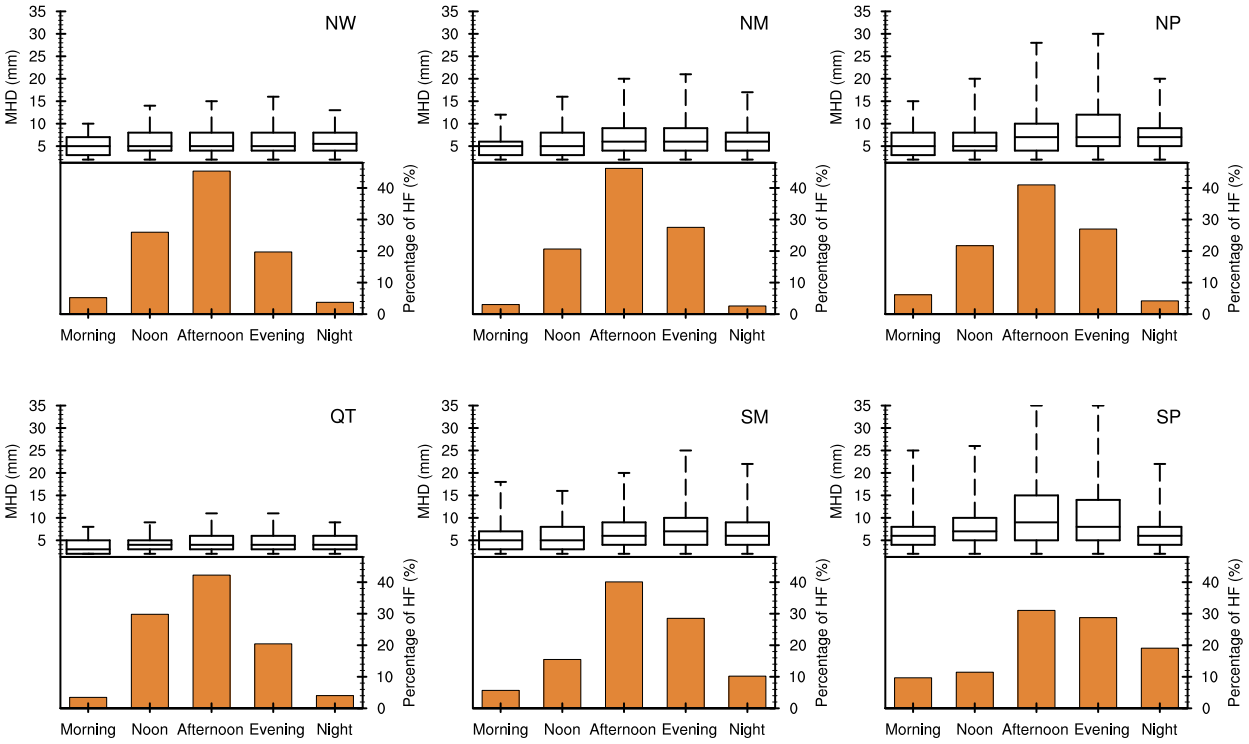

FIG. 6. Diurnal MHD (box plots) and mean percentage HF (bar charts) for the six subareas shown in Fig. 1. Each day was divided into five periods: morning (0800–1059 LT), noon (1100–1359 LT), afternoon (1400–1659 LT), evening (1700–1959 LT), and night (2000–0759 LT). Box plot whiskers indicate the values from the 5th to 95th percentile, the bottom and top of the box are the first (25th percentile) and third (75th percentile) quartiles, respectively, and the band inside the box is the median.

This result might be due to the lower freezing-level height during the evening, such that hailstones would grow larger and an elevated layer of conditionally unstable air would be maintained in SP (X. Chen et al. 2014).

4. Climatology of severe hail

Previous studies (Tuovinen et al. 2009; Allen and Tippett 2015; Burcea et al. 2016; Kahraman et al. 2016) have characterized the climatological features of severe hail in other parts of the world; however, very few such studies have been performed in China (Xie et al. 2010). In the present study, the climatology of annual and diurnal severe hail (MHD $\geq$ 20 mm) events were investigated, using the 3447 severe hail records among the 64 815 MHD records (5.32%) from 1446 stations (Table 1); these records revealed a different pattern than that produced from the records of MHD $\geq$ 2 mm events.

Severe hail showed large spatial differences among the six subareas, with two concentrated areas of severe hail (Fig. 7), such as the zone between the plains areas and mountainous areas in northern and southern China, where there is always a steep terrain shift between mountains and plains (Fig. 1).

Most severe hail occurred between May and September in NW, NM, NP, and QT; however, in southern China, including SM and SP, the most active month with a peak of severe hail was April (Fig. 8). From March to May, more than 70% of severe hail events occurred in SM and SP. The severe HF peaks were delayed 1 month in NM and SP, and the start of severe HF records was delayed by 1 month in NM, NP, and QT when compared with all hail records (Fig. 5). The annual MHD distribution of severe hail exhibited a positive relationship with HF in all subareas, although the 20th, 50th, and 80th percentiles of CDF trends were more complicated because of the limited numbers of severe hail records in all subareas (Fig. 8). There was one peak for the MHD at the 80th percentile of the CDF trend line in May, in which all hail records in SP peaked (Fig. 5) at 50 mm.

Severe hail tended to show similar diurnal cycle patterns (Fig. 9) to all hail records. Severe hail also occurred more frequently in daytime than at night for all six subareas, although the distributions were flat from afternoon through evening in southern China. The

Unauthenticated | Downloaded 05/15/25 05:17 PM UTC

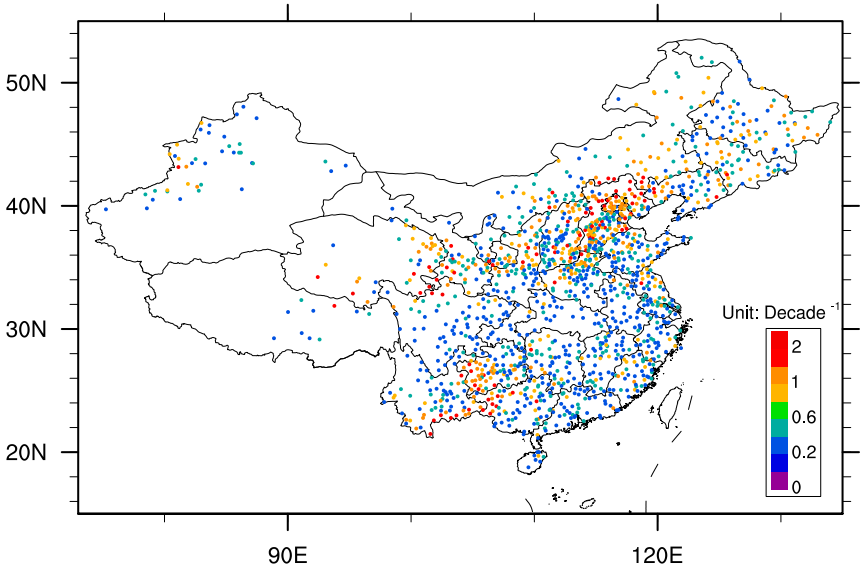

FIG. 7. As in Fig. 2a, but for MHD ≥ 20 mm.

severe hail frequency peaked in the afternoon for all subareas, except for the broad peak from afternoon through evening for SM and SP. In the morning, severe hail was rare (less than 10% of hail occurrence in all subareas), perhaps partly because this is an unfavorable time for convective storms. Severe hail represented a lower percentage of HF in the morning than at night in all subareas, which is consistent with previous studies of hail, which found that severe hail typically occurred more frequently in the afternoon and early evening than in the morning, globally (Schuster et al. 2005; Zhang et al. 2008; Tuovinen et al. 2009). The MHD of severe hail did not present an obvious trend because of the limited number of severe hail records, particularly during the morning and at night.

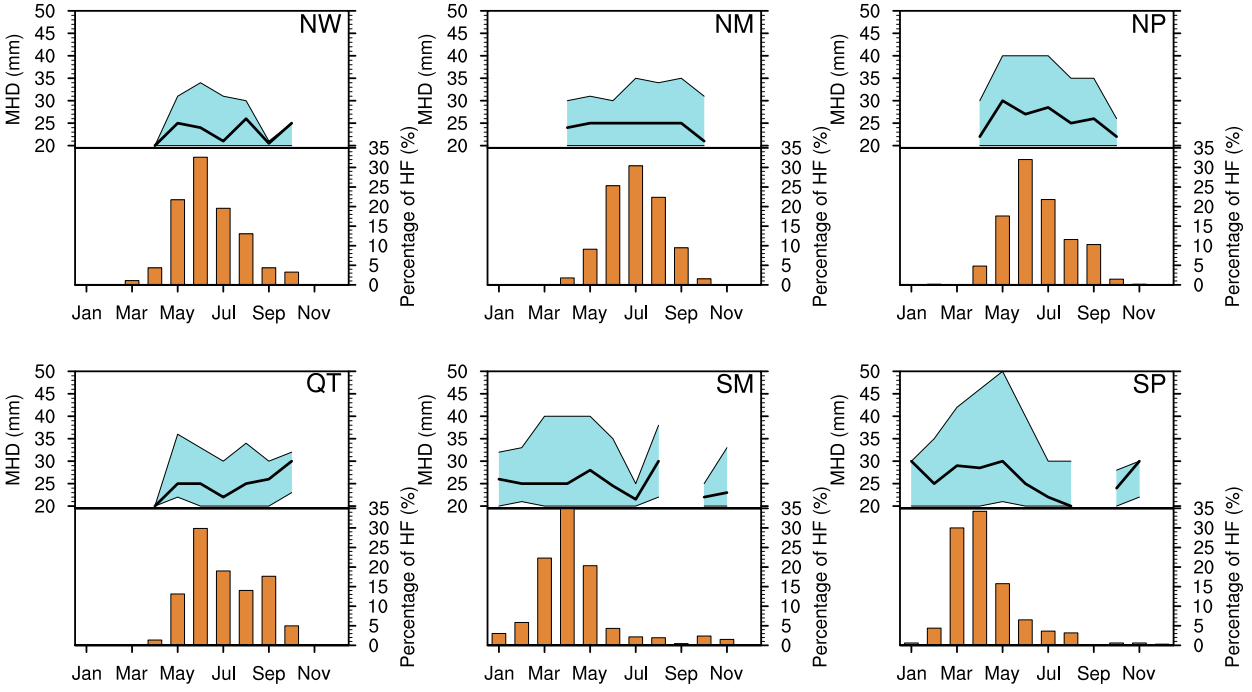

FIG. 8. As in Fig. 5, but for MHD ≥ 20 mm.

Unauthenticated | Downloaded 05/15/25 05:17 PM UTC

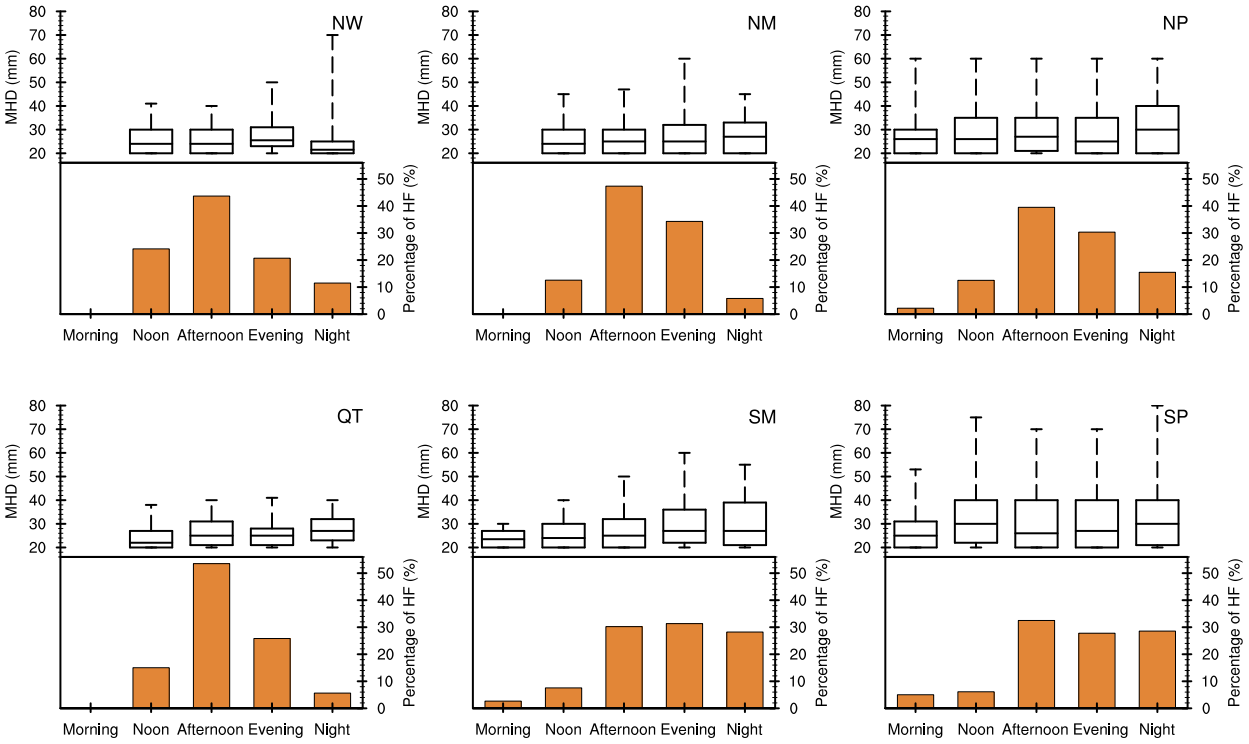

FIG. 9. As in Fig. 6, but for MHD ≥ 20 mm.

5. Conclusions

The current study further extends the hail climatology of China, with thousands of stations during 1980–2015, as compared with hundreds of stations until 2012 (Li et al. 2016). In addition, more detailed hail information, that is, HF and MHD instead of hail day frequency (Liu and Tang 1966; Zhang et al. 2008; Xie et al. 2008; Li et al. 2016; Ni et al. 2016), was analyzed in this study. This meteorological station-based dataset of hail records from the NMIC, including 2254 stations providing 64 815 MHD records and 87 498 hail occurrence records, has allowed an examination of the climatology of hail, including severe hail, during 1980–2015. The relatively short 36-yr data record used here for six subareas permitted a limited examination of severe hail, with a careful investigation of the entire hail record because of the relatively high quality and dense distribution of the stations in China, especially in eastern China. This study analyzed the spatial distribution of HF and MHD from the perspective of the annual and diurnal hail cycles.

The spatial patterns strongly suggested a positive correlation between elevation and HF, and a negative correlation between elevation and MHD. Higher mean HF values and lower mean MHD values always occurred at higher elevations, for example, in NM and NE, and SM and SP, respectively. June was the peak month for HF among all hail records in NW, NM, NP, and QT, whereas April and March were the peak months in SM and SP. The annual distribution of MHD among all hail records roughly followed the annual distribution of HF in all subareas except QT and was delayed by 1 or 2 months in NM, NP, SM, and SP relative to the peak month of HF. The highest percentage of HF occurred in the afternoon, and the highest 90% CDF of MHD occurred in the evening in the diurnal cycle.

There was a remarkable difference in the spatial distribution between smaller hail records (HF maximized in the QT region) and severe hail. Severe hail mainly occurred along the boundaries between SM and SP and between NM and NP in the mountainous regions. Southern China, including SM and SP, experienced severe hail earlier in a year, between March and May, which is consistent among all hail records. In the diurnal cycle, the highest percentage of severe hail HF values occurred during the afternoon in all subareas except SM, where evening was the peak period. Severe hail occurred more frequently at night than in the morning; however, the number of severe hail records was limited in all subareas. Using only 5.32% of all hail size records during 1980–2015, this study also showed that severe hail could occur in any part of China. The distribution of severe hail records is highly dependent on orography, which is consistent with the findings in the peak areas for

Unauthenticated | Downloaded 05/15/25 05:17 PM UTC

severe hail occurrence in regions across Europe, with a maximum in central Europe (Punge and Kunz 2016), and the United States, with a maximum in the central plains (Cintineo et al. 2012; Allen and Tippett 2015).

This study is the first step in improving our understanding of hail climatology using recently revealed comprehensive MHD data combined with HF data in China. It should play an important role in characterizing the regional distribution of hail over China. It also supplements the global hail climatology distribution and provides statistically robust data to enable comparisons of satellite datasets and the results of global model analyses. However, little attention has previously been paid to the mechanisms that produce the distribution of hail over China, and it is therefore difficult to explain the present results from a cause-and-effect perspective at this stage. For example, the environmental conditions that favor hailstorms likely play different roles in the occurrence and growth of hail in different subareas. Therefore, further research should be considered to address this issue.

Acknowledgments. This study was supported by the National Natural Science Foundation of China (Grants 41330421 and 41461164006). The authors also thank the editor and anonymous reviewers, whose valuable comments and suggestions significantly improved this article.

REFERENCES

Allen, J. T., and M. K. Tippett, 2015: The characteristics of United States hail reports: 1955–2014. *Electron. J. Severe Storms Meteor.*, **10** (3), http://www.ejssm.org/ojs/index.php/ejssm/article/view/149/104.

——, and E. R. Allen, 2016: A review of severe thunderstorms in Australia. *Atmos. Res.*, **178–179**, 347–366, https://doi.org/10.1016/j.atmosres.2016.03.011.

——, M. K. Tippett, Y. Kaheil, A. H. Sobel, C. Lepore, S. Nong, and A. Muehlbauer, 2017: An extreme value model for United States hail size. *Mon. Wea. Rev.*, **145**, 4501–4519, https://doi.org/10.1175/MWR-D-17-0119.1.

Brooks, H. E., and N. Dotzek, 2008: The spatial distribution of severe convective storms and an analysis of their secular changes. *Climate Extremes and Society*, H. F. Diaz and R. Murnane, Eds., Cambridge University Press, 35–53.

Burcea, S., R. Cică, and R. Bojariu, 2016: Hail climatology and trends in Romania: 1961–2014. *Mon. Wea. Rev.*, **144**, 4289–4299, https://doi.org/10.1175/MWR-D-16-0126.1.

Cao, Z., 2008: Severe hail frequency over Ontario, Canada: Recent trend and variability. *Geophys. Res. Lett.*, **35**, L14803, https://doi.org/10.1029/2008GL034888.

Cecil, D. J., and C. B. Blankenship, 2012: Toward a global climatology of severe hailstorms as estimated by satellite passive microwave imagers. *J. Climate*, **25**, 687–703, https://doi.org/10.1175/JCLI-D-11-00130.1.

Changnon, S. A., 1978: The climatology of hail in North America. *Hail: A Review of Hail Science and Hail Suppression*, *Meteor. Monogr.*, No. 38, Amer. Meteor. Soc., 107–128.

——, and D. Changnon, 2000: Long-term fluctuations in hail incidences in the United States. *J. Climate*, **13**, 658–664, https://doi.org/10.1175/1520-0442(2000)013<0658:LTFIHI>2.0.CO;2.

Chen, G., R. Yoshida, W. Sha, T. Iwasaki, and H. Qin, 2014: Convective instability associated with the eastward-propagating rainfall episodes over eastern China during the warm season. *J. Climate*, **27**, 2331–2339, https://doi.org/10.1175/JCLI-D-13-00443.1.

Chen, X., K. Zhao, and M. Xue, 2014: Spatial and temporal characteristics of warm season convection over Pearl River Delta region, China, based on 3 years of operational radar data. *J. Geophys. Res. Atmos.*, **119**, 12 447–12 465, https://doi.org/10.1002/2014JD021965.

China Meteorological Administration, 2007: Specifications for surface meteorological observation. *Observation of Weather Phenomenon*, China Meteorological Press, 21–27.

——, 2016: Chinese meteorological disasters. *Yearbook 2016*, China Meteorological Press, 25–38.

Cintineo, J. L., T. M. Smith, V. Lakshmanan, H. E. Brooks, and K. L. Ortega, 2012: An objective high-resolution hail climatology of the contiguous United States. *Wea. Forecasting*, **27**, 1235–1248, https://doi.org/10.1175/WAF-D-11-00151.1.

Dennis, E. J., and M. R. Kumjian, 2017: The impact of vertical wind shear on hail growth in simulated supercells. *J. Atmos. Sci.*, **74**, 641–663, https://doi.org/10.1175/JAS-D-16-0066.1.

Dotzek, N., P. Groenemeijer, B. Feuerstein, and A. M. Holzer, 2009: Overview of ESSL's severe convective storms research using the European Severe Weather Database ESWD. *Atmos. Res.*, **93**, 575–586, https://doi.org/10.1016/j.atmosres.2008.10.020.

Grant, L. D., and S. C. van den Heever, 2014: Microphysical and dynamical characteristics of low-precipitation and classic supercells. *J. Atmos. Sci.*, **71**, 2604–2624, https://doi.org/10.1175/JAS-D-13-0261.1.

Guan, Y., F. Zheng, P. Zhang, and C. Qin, 2015: Spatial and temporal changes of meteorological disasters in China during 1950–2013. *Nat. Hazards*, **75**, 2607–2623, https://doi.org/10.1007/s11069-014-1446-3.

Hand, W. H., and G. Cappelluti, 2011: A global hail climatology using the UK Met Office convection diagnosis procedure (CDP) and model analyses. *Meteor. Appl.*, **18**, 446–458, https://doi.org/10.1002/met.236.

Hohl, R., H. H. Schiesser, and D. Aller, 2002: Hailfall: The relationship between radar-derived hail kinetic energy and hail damage to buildings. *Atmos. Res.*, **63**, 177–207, https://doi.org/10.1016/S0169-8095(02)00059-5.

Jin, H.-G., H. Lee, J. Lkhamjav, and J.-J. Baik, 2017: A hail climatology in South Korea. *Atmos. Res.*, **188**, 90–99, https://doi.org/10.1016/j.atmosres.2016.12.013.

Johns, R. H., and C. A. Doswell III, 1992: Severe local storms forecasting. *Wea. Forecasting*, **7**, 588–612, https://doi.org/10.1175/1520-0434(1992)007<0588:SLSF>2.0.CO;2.

Kahraman, A., S. Tilev-Tanriover, M. Kadioglu, D. M. Schultz, and P. M. Markowski, 2016: Severe hail climatology of Turkey. *Mon. Wea. Rev.*, **144**, 337–346, https://doi.org/10.1175/MWR-D-15-0337.1.

Kim, C., and X. Ni, 2014: Climatology of hail in North Korea (in Chinese). *Beijing Huagong Daxue Xuebao*, **51**, 437–443.

Li, C., Y. Li, and X. Jiang, 2015: Statistical characteristics of the inter-monthly variation of the Sichuan Basin vortex and the distribution of daily precipitation (in Chinese). *Chin. J. Atmos. Sci.*, **39**, 1191–1203.

Li, M., Q. Zhang, and F. Zhang, 2016: Hail day frequency trends and associated atmospheric circulation patterns over China

Unauthenticated | Downloaded 05/15/25 05:17 PM UTC

during 1960–2012. *J. Climate*, **29**, 7027–7044, https://doi.org/10.1175/JCLI-D-15-0500.1.

Li, X., X. Guo, and D. Fu, 2013: TRMM-retrieved cloud structure and evolution of MCSs over the northern South China Sea and impacts of CAPE and vertical wind shear. *Adv. Atmos. Sci.*, **30**, 77–88, https://doi.org/10.1007/s00376-012-2055-2.

——, Q. Zhang, and H. Xue, 2017: The role of initial cloud condensation nuclei concentration in hail using the WRF NSSL 2-moment microphysics scheme. *Adv. Atmos. Sci.*, **34**, 1106–1120, https://doi.org/10.1007/s00376-017-6237-9.

Liu, Q. G., and M. C. Tang, 1966: Climatological characteristics of hail in China (in Chinese). *Acta Geogr. Sin.*, **32**, 48–65.

Martins, J. A., and Coauthors, 2017: Climatology of destructive hailstorms in Brazil. *Atmos. Res.*, **184**, 126–138, https://doi.org/10.1016/j.atmosres.2016.10.012.

Nelson, S. P., 1983: The influence of storm flow structure on hail growth. *J. Atmos. Sci.*, **40**, 1965–1983, https://doi.org/10.1175/1520-0469(1983)040<1965:TIOSFS>2.0.CO;2.

Ni, X., C. Liu, Q. Zhang, and D. J. Cecil, 2016: Properties of hail storms over China and the United States from the Tropical Rainfall Measuring Mission. *J. Geophys. Res. Atmos.*, **121**, 12 031–12 044, https://doi.org/10.1002/2016JD025600.

——, Q. Zhang, C. Liu, X. Li, T. Zou, J. Lin, H. Kong, and Z. Ren, 2017: Decreased hail size in China since 1980. *Sci. Rep.*, **7**, 10913, https://doi.org/10.1038/s41598-017-11395-7.

Punge, H. J., and M. Kunz, 2016: Hail observations and hailstorm characteristics in Europe: A review. *Atmos. Res.*, **176–177**, 159–184, https://doi.org/10.1016/j.atmosres.2016.02.012.

Schuster, S. S., J. B. Russell, and M. S. Speer, 2005: A hail climatology of the greater Sydney area and New South Wales, Australia. *Int. J. Climatol.*, **25**, 1633–1650, https://doi.org/10.1002/joc.1199.

Thielen, J., and A. Gadian, 1997: Influence of topography and urban heat island effects on the outbreak of convective storms under unstable meteorological conditions: A numerical study. *Meteor. Appl.*, **4**, 139–149, https://doi.org/10.1017/S1350482797000303.

Tuovinen, J., A. Punkka, J. Rauhala, H. Hohti, and D. M. Schultz, 2009: Climatology of severe hail in Finland: 1930–2006. *Mon. Wea. Rev.*, **137**, 2238–2249, https://doi.org/10.1175/2008MWR2707.1.

Vinet, F., 2001: Climatology of hail in France. *Atmos. Res.*, **56**, 309–323, https://doi.org/10.1016/S0169-8095(00)00082-X.

Xie, B., Q. Zhang, and Y. Wang, 2008: Trends in hail in China during 1960–2005. *Geophys. Res. Lett.*, **35**, L13801, https://doi.org/10.1029/2008GL034067.

——, ——, and ——, 2010: Observed characteristics of hail size in four regions in China during 1980–2005. *J. Climate*, **23**, 4973–4982, https://doi.org/10.1175/2010JCLI3600.1.

Yu, Y., J. Li, J. Xie, and C. Liu, 2016: Climatic characteristics of thunderstorm days and the influence of atmospheric environment in northwestern China. *Nat. Hazards*, **80**, 823, https://doi.org/10.1007/s11069-015-1999-9.

Zhang, C., Q. Zhang, and Y. Wang, 2008: Climatology of hail in China: 1961–2005. *J. Appl. Meteor. Climatol.*, **47**, 795–804, https://doi.org/10.1175/2007JAMC1603.1.

Zhang, Q., X. Ni, and F. Zhang, 2017: Decreasing trend in severe weather occurrence over China during the past 50 years. *Sci. Rep.*, **7**, 42310, https://doi.org/10.1038/srep42310.

Zheng, D., Y. Zhang, Q. Meng, L. Chen, and J. Dan, 2016: Climatology of lightning activity in South China and its relationships to precipitation and convective available potential energy. *Adv. Atmos. Sci.*, **33**, 365, https://doi.org/10.1007/s00376-015-5124-5.

Ziegler, C. S., P. S. Ray, and N. C. Knight, 1983: Hail growth in an Oklahoma multicell storm. *J. Atmos. Sci.*, **40**, 1768–1791, https://doi.org/10.1175/1520-0469(1983)040<1768:HGIAOM>2.0.CO;2.

Unauthenticated | Downloaded 05/15/25 05:17 PM UTC